Electronic Supplementary Information (ESI)

The study process on the energy transfer mechanism of $Ce^{3+} \rightarrow Eu^{2+}$ ion pair in the CGPO host is illustrated in detail as follows:

In order to validate the energy transfer from Ce^{3+} to Eu^{2+}, we first investigated the decay curves of Ce^{3+} in the CGPO host. The decay curve of CGPO: $9Ce^{3+}$ has been analyzed by curve fitting, as shown in Figure S5a. When Eu^{2+} ions are introduced, the decays deviate from exponential. Figure S5b shows the representative decay curves of Ce^{3+} emission in CGPO: $9Ce^{3+}$, yEu^{2+} (y = 1, 4) samples excited at 314 nm and monitored at 415 nm, which are displayed on a logarithmic intensity scale. It can be observed that the deviation is more evident with the increase of the Eu^{2+} doping content, and the decay of the Ce^{3+} ions become faster and faster attributed to the energy transfer from the Ce^{3+} to Eu^{2+} ions. Since the deviations from exponential decay, the average fluorescence lifetime was defined as following formula:[1]

$$\tau_{avg} = \frac{\int_0^\infty tI(t)dt}{\int_0^\infty I(t)dt} \quad (1)$$

Where $I_{(t)}$ is the fluorescence intensity at time t with normalized initial intensity. The average lifetimes of Ce^{3+} as a function of different Eu^{2+} concentration were calculated and shown in Figure S5c (black line). It can be seen that the lifetime of the Ce^{3+} emission shortens with increasing doping content of Eu^{2+}, which strongly supports the energy transfer from the Ce^{3+} to Eu^{2+} ions. In addition, the energy transfer efficiency from Ce^{3+} to Eu^{2+} was also investigated. Generally, the energy transfer efficiency from a sensitizer to activator can be expressed as the following equation[2-4]

$$\eta_T = 1 - \frac{\tau_S}{\tau_{S0}} \quad (2)$$

Where η_T is the energy transfer efficiency, τ_{S0} and τ_S are the lifetime of the Ce^{3+} sensitizer in the absence and presence of Eu^{2+} ions, respectively. As a consequence, the η_T values from Ce^{3+} to Eu^{2+} in CGPO: $9Ce^{3+}$, yEu^{2+} samples were calculated as a function of y and represented in Figure S4c (blue

line). It can be observed that the energy transfer efficiency increases with increasing Eu^{2+} concentration. However, the increscent rate of the energy transfer efficiency gradually decreases with the increase of Eu^{2+} concentration. These results reveal that the energy transfer from Ce^{3+} to Eu^{2+} has a trend to saturation with a continuous increase of Eu^{2+} concentration due to the fixed Ce^{3+} concentration. The maximum energy transfer efficiency can reach 65%. The above results indicate that the energy transfer from Ce^{3+} to Eu^{2+} is efficient.

On the basis of Dexter's energy transfer expressions of multipolar interaction and Reisfeld's approximation, the following relation can be given as [5, 6]

$$\ln\frac{\eta_{S0}}{\eta_S} \propto C \quad (3)$$

$$\frac{\eta_{S0}}{\eta_S} \propto C^{n/3} \quad (4)$$

where η_{S0} and η_S are the luminescence quantum efficiencies of Ce^{3+} in the absence and presence of Eu^{2+}, respectively; C is the total doping concentration of the Ce^{3+} and Eu^{2+} ions; eq 3 corresponds to the exchange interaction and eq 4 with n = 6, 8, and 10 corresponds to dipole-dipole, dipole-quadrupole, and quadrupole-quadrupole interactions, respectively. The value of η_{S0}/η_S can be approximately estimated from the related lifetime's ratio (τ_{S0}/τ_S). Thus, eqs. 3 and 4 can be represented by the following equation:

$$\ln\frac{\tau_{S0}}{\tau_S} \propto C \quad (5)$$

$$\frac{\tau_{S0}}{\tau_S} \propto C^{n/3} \quad (6)$$

The relationships of $\ln(\tau_{S0}/\tau_S) \propto C$ and $(\tau_{S0}/\tau_S) \propto C^{n/3}$ are illustrated in Figure S6, in which a linear behavior was observed only when n = 6, implying that energy transfer from Ce^{3+} to Eu^{2+} occurs via a dipole-dipole mechanism.

1 L. Shi, Y. L. Huang and H. J. Seo, *J. Phys. Chem. A*, 2010, **114**, 6927.

2 (a) W. J. Yang and T. M. Chen, *Appl. Phys. Lett.*, 2006, **88**, 101903; (b) A. Kar, A. Datta and A. Patra, *J. Mater. Chem.*, 2010, **20**, 916.

3 K. H. Kwon, W. B. Im, H. S. Jang, H. S. Yoo and D. Y. Jeon, *Inorg. Chem.*, 2009, **48**, 11525.

4 P. I. Paulose, G. Jose, V. Thomas, N. V. Unnikrishnan and K. R. M. Warrier, *J. Phys. Chem. Solids*, 2003, **64**, 841.

5 D. L. Dexter, *J. Chem. Phys.*, 1953, **21**, 836.

6 G. Blasse, *Philips. Res. Rep.*, 1969, **24**, 131.

Table S1. Structure parameters of $Ca_8Gd_2(PO_4)_6O_2$ and ionic radii (Å) for given coordination number (CN) of Gd^{3+}, Ca^{2+}, Ce^{3+}, Eu^{2+}, Tb^{3+}, Dy^{3+}, and Mn^{2+} ions.

Ion	Space group	Sites	Symmetry	Ionic radius (IR) (Å)	
				CN = 9	CN = 7
Gd^{3+}	Hexagonal $P6_3/m$ (176)	6h	C_s	1.107	1.00
Ca^{2+}		6h/4f	C_s/C_3	1.180	1.06
Ce^{3+}				1.196	1.07
Eu^{2+}				1.300	1.20
Tb^{3+}				1.095	0.98
Dy^{3+}				1.083	0.97
Mn^{2+}				—	0.9

Table S2. Cell parameters of CGPO: A (A = Ce^{3+}, Eu^{2+}, Mn^{2+}, Tb^{3+}, Dy^{3+}) samples at different A concentration.

Sample \ Cell parameter	a = b (Å)	c (Å)	V (Å^3)
CGPO: $1Eu^{2+}$	9.39392	6.87661	525.53
CGPO: $3Eu^{2+}$	9.40563	6.88662	527.61
CGPO: $5Eu^{2+}$	9.41216	6.88948	528.56
CGPO: $3Ce^{3+}$	9.38182	6.87349	523.94
CGPO: $7Ce^{3+}$	9.38722	6.87810	524.90
CGPO: $10Ce^{3+}$	9.39655	6.87974	526.07
CGPO: $3Tb^{3+}$	9.36707	6.86741	521.83
CGPO: $5Tb^{3+}$	9.36069	6.86105	521.75
CGPO: $10Tb^{3+}$	9.34256	6.85782	518.38
CGPO: $4Mn^{2+}$	9.37956	6.86953	523.39
CGPO: $7Mn^{2+}$	9.37870	6.86938	523.28
CGPO: $10Mn^{2+}$	9.37743	6.86739	522.99
CGPO: $9Ce^{3+}$, $2Dy^{3+}$	9.36997	6.86817	522.21
CGPO: $9Ce^{3+}$, $4Dy^{3+}$	9.36899	6.86557	521.91
CGPO: $9Ce^{3+}$, $8Dy^{3+}$	9.36427	6.85924	520.9

Table S3. Quantum yields (QYs) and chromaticity coordinates of the Ce^{3+} and/or Eu^{2+} doped CGPO samples under UV excitation.

CGPO	Quantum yields (%)
	λ_{ex} = 314 nm
CGPO: $1Ce^{3+}$	66
CGPO: $3Ce^{3+}$	72
CGPO: $4Ce^{3+}$	76
CGPO: $5Ce^{3+}$	82
CGPO: $7Ce^{3+}$	84
CGPO: $9Ce^{3+}$	88 (0.166, 0.117)
CGPO: $10Ce^{3+}$	85
CGPO: $15Ce^{3+}$	83
	λ_{ex} = 300 nm
CGPO: $1Eu^{2+}$	12
CGPO: $3Eu^{2+}$	17
CGPO: $4Eu^{2+}$	19 (0.161, 0.106)
CGPO: $5Eu^{2+}$	18
CGPO: $6Eu^{2+}$	16
CGPO: $7Eu^{2+}$	14
CGPO: $8Eu^{2+}$	13
CGPO: $10Eu^{2+}$	9
CGPO: $15Eu^{2+}$	8
	λ_{ex} = 314 nm
CGPO : $9Ce^{3+}$	88
CGPO: $9Ce^{3+}$, $1Eu^{2+}$	60
CGPO: $9Ce^{3+}$, $3Eu^{2+}$	33.5 (0.165, 0.108)
CGPO: $9Ce^{3+}$, $4Eu^{2+}$	28
CGPO: $9Ce^{3+}$, $5Eu^{2+}$	22
CGPO: $9Ce^{3+}$, $6Eu^{2+}$	22
CGPO: $9Ce^{3+}$, $7Eu^{2+}$	20
CGPO: $9Ce^{3+}$, $8Eu^{2+}$	16
CGPO: $9Ce^{3+}$, $9Eu^{2+}$	14

Table S4. CIE chromaticity coordinates (x, y) of the CGPO: Ce^{3+}, Tb^{3+}, Dy^{3+}, Mn^{2+} under low voltage electron beam (Accelerating Voltage = 3.5 kV; Filament Current = 91 mA)

point	sample	Chromaticity coordinates (x, y)
1	CGPO: $9Ce^{3+}$	(0.190, 0.162)
2	CGPO: $9Ce^{3+}$, $1Tb^{3+}$	(0.196, 0.199)
3	CGPO: $9Ce^{3+}$, $3Tb^{3+}$	(0.209, 0.269)
4	CGPO: $9Ce^{3+}$, $7Tb^{3+}$	(0.241, 0.459)
5	CGPO: $9Tb^{3+}$	(0.283, 0.520)
6	CGPO: $9Ce^{3+}$, $4Dy^{3+}$	(0.230, 0.213)
7	CGPO: $9Ce^{3+}$, $8Dy^{3+}$	(0.265, 0.252)
8	CGPO: $9Dy^{3+}$	(0.352, 0.371)
9	CGPO: $9Ce^{3+}$, $5Mn^{2+}$	(0.219, 0.219)
10	CGPO: $9Ce^{3+}$, $10Mn^{2+}$	(0.253, 0.279)
11	CGPO: $9Ce^{3+}$, $18Mn^{2+}$	(0.286, 0.332)
12	CGPO: $7Mn^{2+}$	(0.343, 0.473)

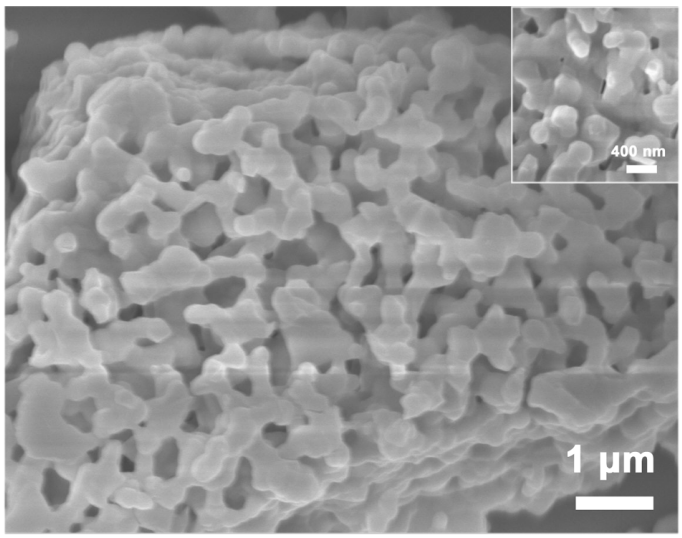

Figure S1. SEM image of CGPO: Ce^{3+}, Eu^{2+} sample.

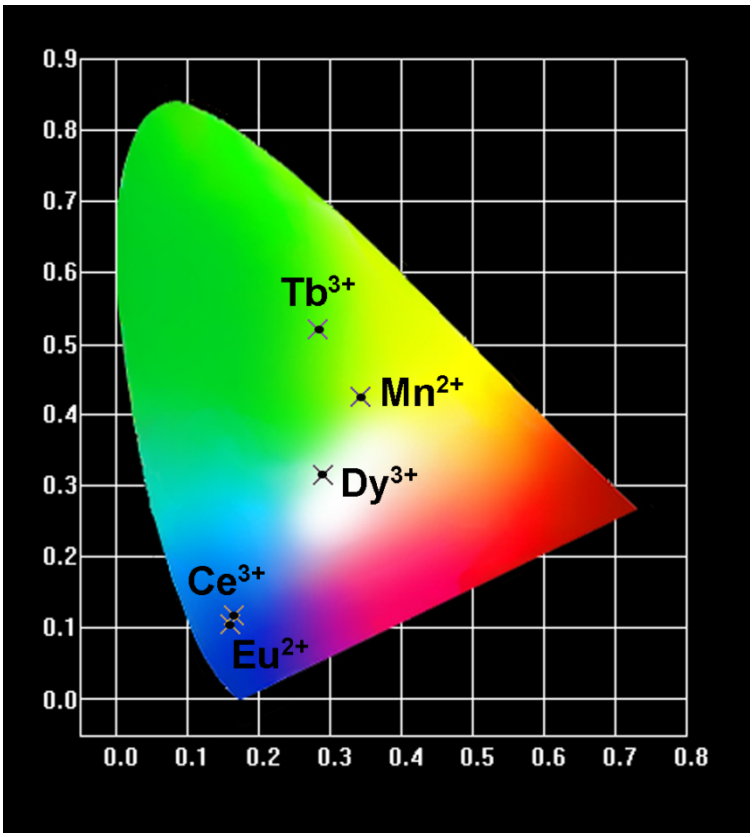

Figure S2. The CIE chromaticity diagram for CGPO: $9Ce^{3+}$ and CGPO: $4Eu^{2+}$, CGPO: $9Tb^{3+}$, CGPO: $3Dy^{3+}$, CGPO: $5Mn^{2+}$samples.

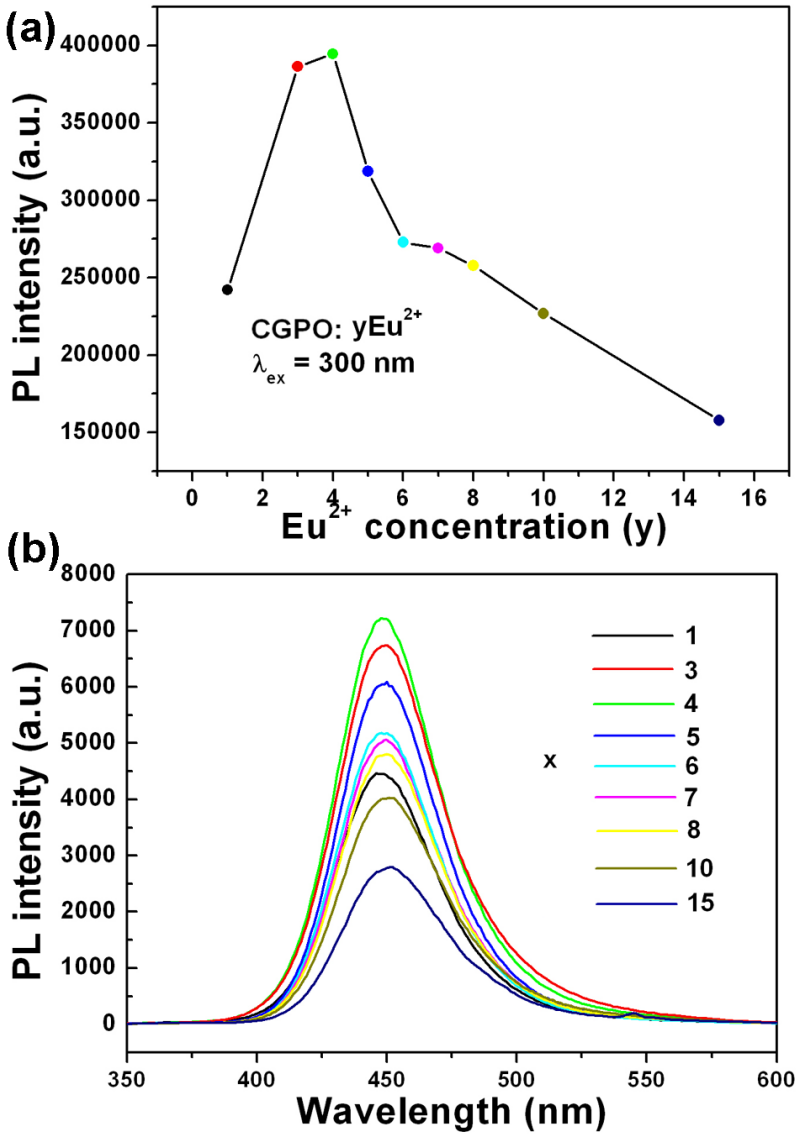

Figure S3. (a) The PL intensity of CGPO: yEu^{2+} samples as a function of the Eu^{2+} doping concentration (y). (b) The variation of PL spectra for CGPO: yEu^{2+} samples with Eu^{2+} concentration (y = 1-15) under 300 nm excitation.

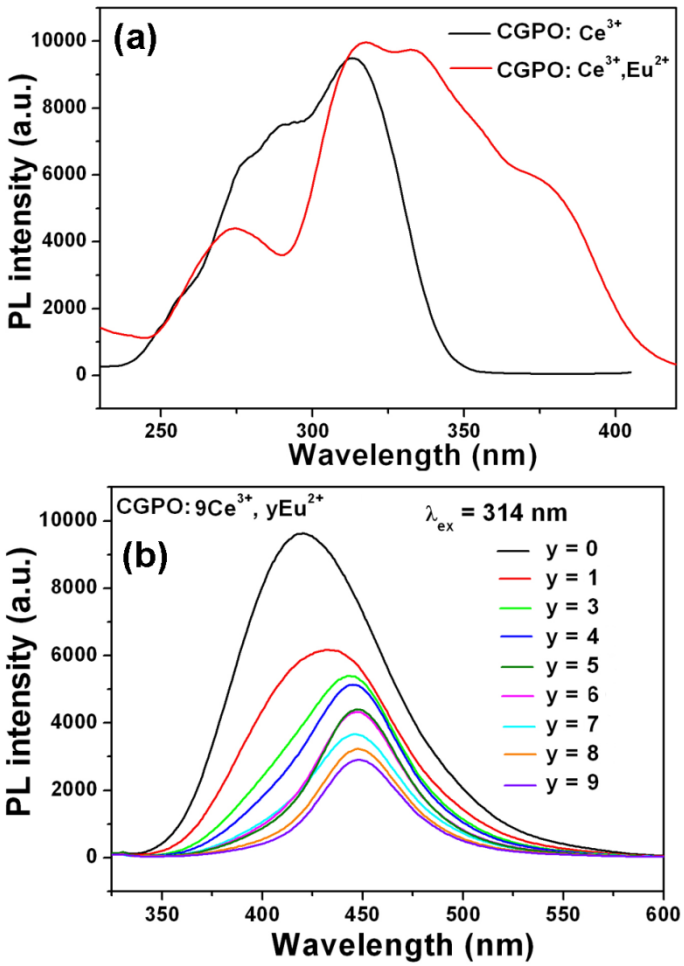

Figure S4. (a) The PLE spectra for CGPO: Ce^{3+} (black line) (λ_{em} = 415 nm) and CGPO: Ce^{3+}, Eu^{2+} (λ_{em} = 452 nm) (red line) samples. (b) PL spectra for CGPO: $9Ce^{3+}$, yEu^{2+} excited at 314 nm (y = 0-9).

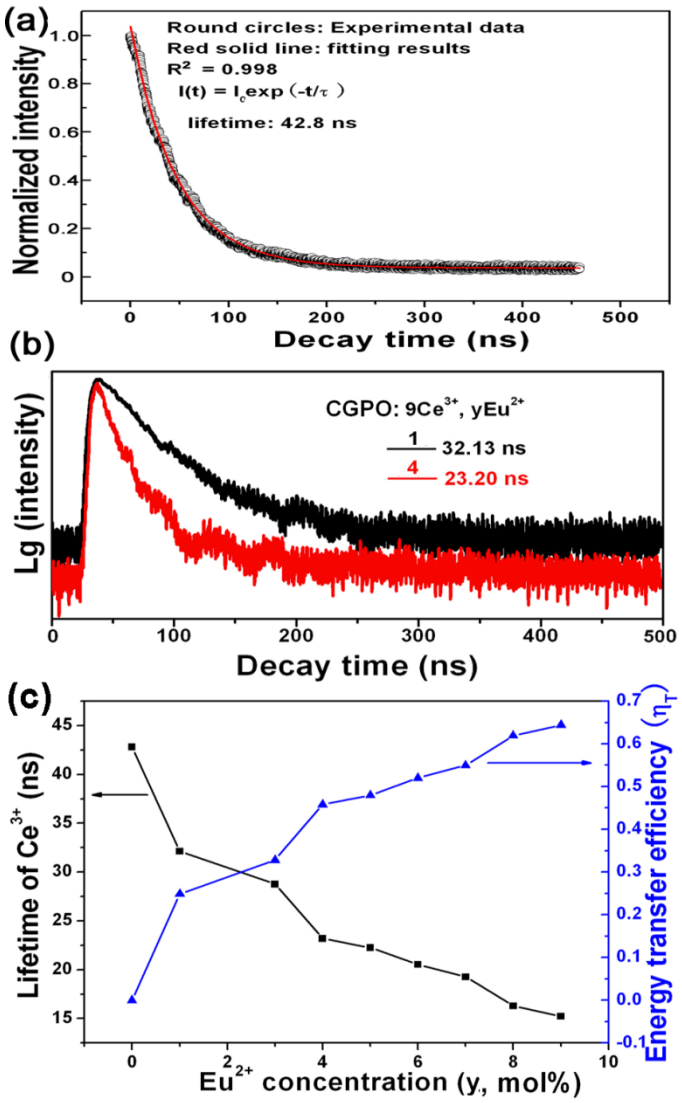

Figure S5. (a) Photoluminescence decay curve of Ce^{3+} emission in CGPO: $9Ce^{3+}$ and curve-fitting under excitation at 313 nm, monitored at 415 nm. (b) Representative photoluminescence decay curves of Eu^{2+} in CGPO: $9Ce^{3+}$, yEu^{2+} (y = 1, 4) displayed on a logarithmic intensity scale (excited at 314nm, monitored at 415nm). (c) Dependence of the energy transfer efficiency (η_T) and the fluorescence lifetime of Ce^{3+} on Eu^{2+} content (y, mol%).

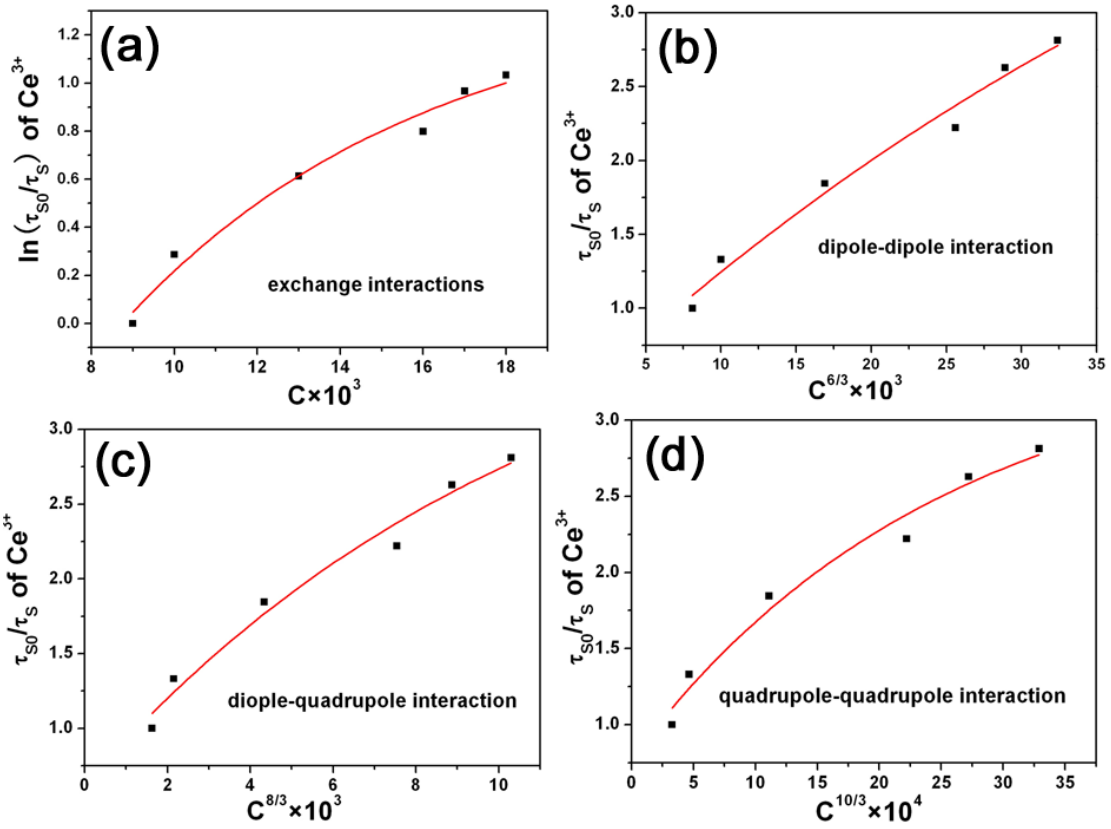

Figure S6. (a) Dependence of $\ln(\tau_{S0}/\tau_S)$ of Ce^{3+} on C; and τ_{S0}/τ_S of Ce^{3+} on (b) $C^{6/3}$, (c) $C^{8/3}$ and (d) $C^{10/3}$.

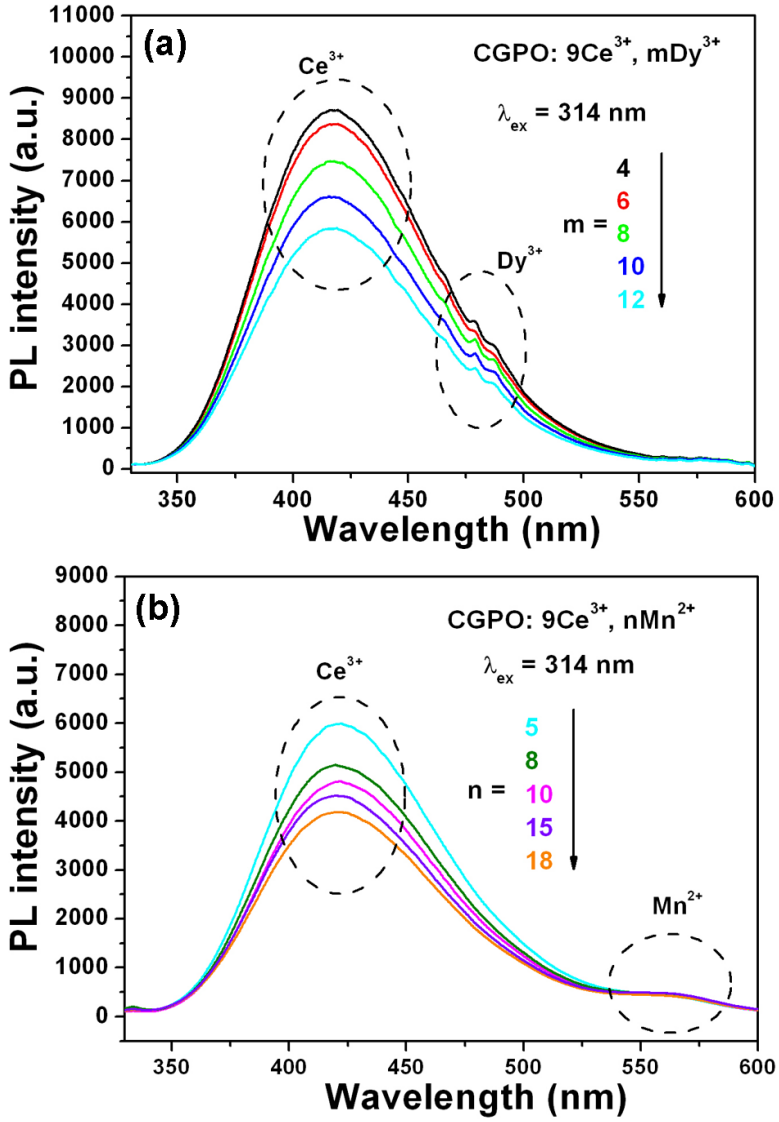

Figure S7. Representative PL spectra for (a) CGPO: $9Ce^{3+}$, mDy^{3+} (m = 4, 6, 8, 10, 12) and (b) CGPO: $9Ce^{3+}$, nMn^{2+} (n = 5, 8, 10, 15, 18) under 314 nm UV excitation.

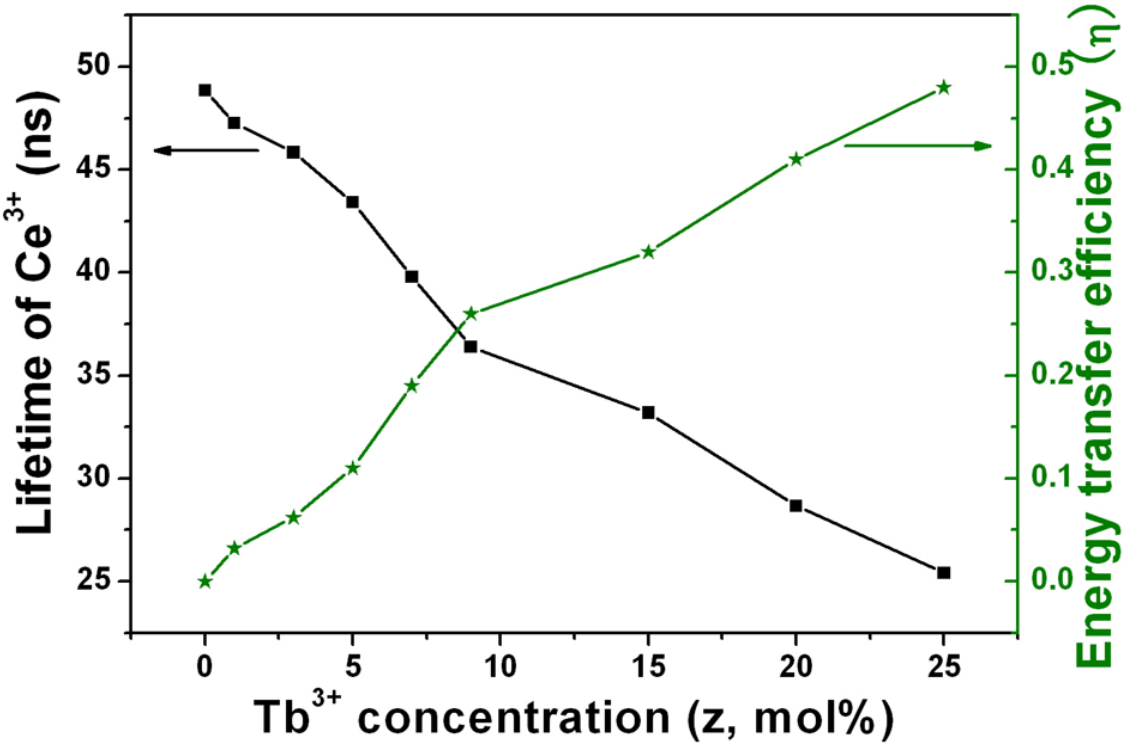

Figure S8. Dependence of the energy transfer efficiency (η) and the fluorescence lifetime of Ce^{3+} on Tb^{3+} content (z, mol%).

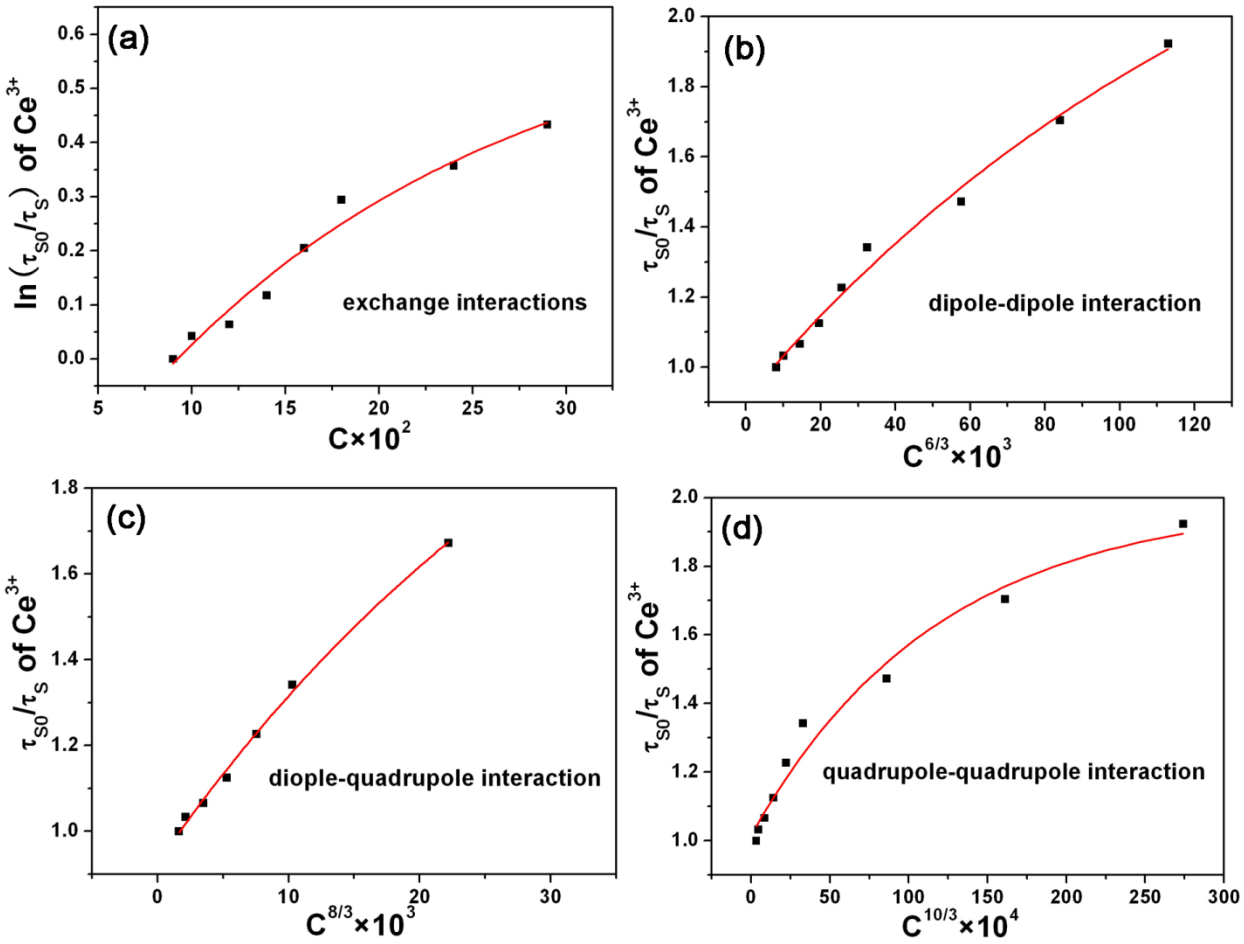

Figure S9. Dependence of (a) $\ln(\tau_{S0}/\tau_S)$ of Ce^{3+} on C; and τ_{S0}/τ_S of Ce^{3+} on (b) $C^{6/3}$, (c) $C^{8/3}$ and (d) $C^{10/3}$.

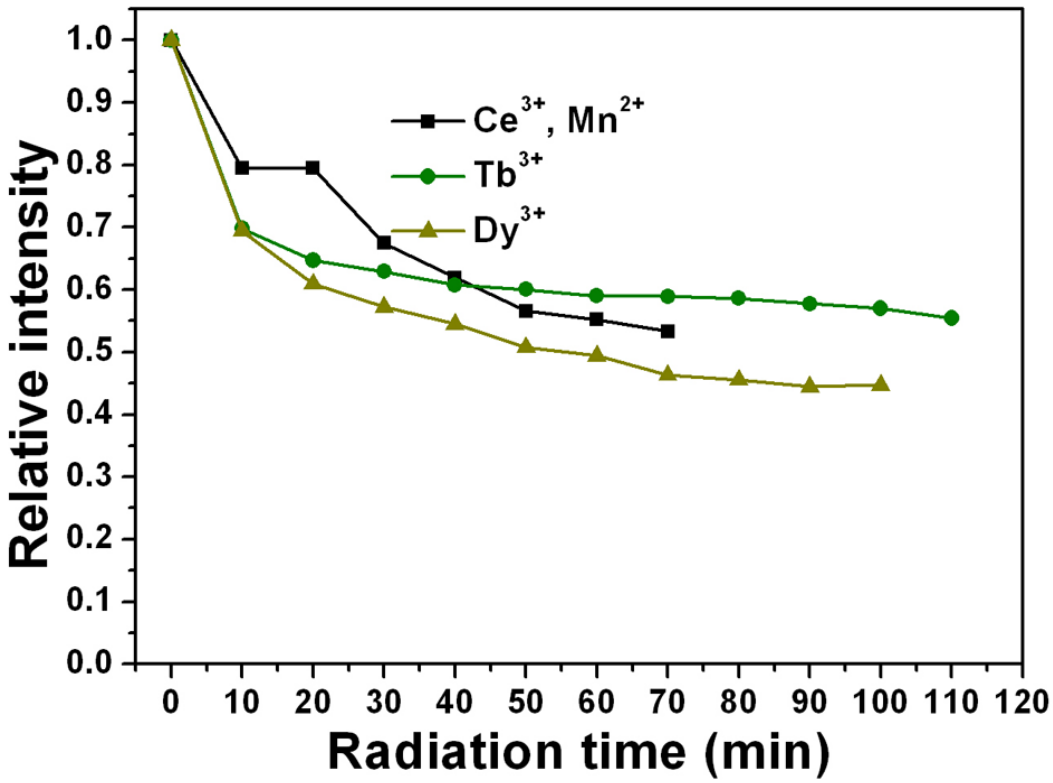

Figure S10. Dependence of relative CL intensity for the representative CGPO: Ce^{3+}, Mn^{2+}, CGPO: Tb^{3+}, and CGPO: Dy^{3+} samples on the radiation time under the accelerating voltage = 3.5kV, filament current = 90 mA electron beam excitation.